12th International Symposium on Turbulence and Shear Flow Phenomena (TSFP12)
Osaka, Japan (Online), July 19-22, 2022

ON THE NATURE OF THE TURBULENT/TURBULENT INTERFACE

Oliver R.H. Buxton
Department of Aeronautics
Imperial College London, UK
o.buxton@imperial.ac.uk

Krishna S. Kankanwadi
Department of Aeronautics
Imperial College London, UK
krishna.kankanwadi12@imperial.ac.uk

ABSTRACT

We perform combined PIV and PLIF experiments to investigate the nature of the interface between two adjacent streams of fully-developed turbulence; the turbulent/turbulent interface (TTI). For the first time we definitively prove the existence of the TTI, something that had been previously questioned for cases where the intensity of the turbulence in both streams is comparable. We then examine the dominant physics in the TTI. Unlike for turbulent/non-turbulent interfaces viscosity does not play an important role and the inertial vortex stretching term is dominant in producing the discontinuity in enstrophy that is characteristic of the TTI. We show that the particular organisation of the small-scale turbulent strain rate and vorticity in the TTI is responsible for driving this vortex stretching and show that freestream turbulence diminishes the rate of entrainment into the primary flow relative to a non-turbulent freestream.

INTRODUCTION

The spatio-temporal processes by which turbulent bodies of fluid expand into the background fluid with advected distance, such as the growth of a volcanic plume in the atmosphere, are collectively known as entrainment. The rate, and process, by which entrainment occurs is governed by the turbulent dynamics within an interfacial layer adjacent to the outermost boundary between the two regions of fluid. In the special case where the background fluid is non-turbulent this layer is known as the turbulent/non-turbulent interface (TNTI). The nature of the TNTI is best explained by examining the behaviour of the terms of the enstrophy ($\omega^2/2$) transport equation

$$\frac{\mathrm{D}}{\mathrm{D}t}\frac{\omega^2}{2} = \underbrace{\omega_i s_{ij} \omega_j}_{\text{vorticity stretching}} + \underbrace{\nu \frac{\partial(\omega^2/2)}{\partial x_j \partial x_j}}_{\text{viscous diffusion}} + \underbrace{\nu \left(\frac{\partial \omega_i}{\partial x_j}\right)^2}_{\text{viscous dissipation}} \quad (1)$$

where ω_i are the components of the vorticity vector and s_{ij} is the strain-rate tensor. A key distinguishing feature of turbulent flows is that they are vortical, i.e. $\omega^2 = |\nabla \times u|^2 \neq 0$, whereas non-turbulent flow is usually irrotational, $\omega^2 = 0$. Accordingly, the outermost boundary between the turbulent and non-turbulent fluid, the irrotational boundary, is an iso-surface of $\omega^2 = 0$. The only non-zero source term in (1) at the irrotational boundary is therefore the viscous diffusion term hence Corrsin & Kistler (1955) postulated the existence of a thin viscous layer at the outer edge of the TNTI, whose thickness ought to scale with the Kolmogorov length scale $\eta = (\nu^3/\varepsilon)^{1/4}$, with ε the dissipation rate of turbulent kinetic energy. This intuition, and scaling has since been confirmed experimentally (Holzner & Lüthi, 2011).

However, the majority of environmental and industrial flows exist within a turbulent background meaning that entrainment takes place between two adjacent streams of turbulent fluid, e.g. between the volcanic plume and the (turbulent) atmospheric boundary layer. We refer to this as turbulent/turbulent entrainment (TTE) and in this case the intuition of Corrsin & Kistler (1955) breaks down since $\omega^2 \neq 0$ on both sides of the interface between the two streams of fluid; the turbulent/turbulent interface (TTI). In fact the existence of the TTI has not yet been definitively proven with the review of da Silva et al. (2014) suggesting that the TTI (if it exists) is likely to "break down" when the turbulence intensity becomes comparable on both sides of the interface. In this paper we prove the existence of the TTI and examine the physics governing TTE since viscous diffusion is no longer the only mechanism by which entrainment can take place in the TTE paradigm.

METHODOLOGY

Examining the physics of TTE requires field velocity data and the ability to identify the TTI and track it through time. Identification of the TTI is not as straightforward as the TNTI due to the fact that $\omega^2 \neq 0$ on both sides of the interface. We thus use a passive scalar, mixed into the primary turbulent flow (a wake produced by a circular cylinder), to identify the extent of the primary flow (wake). In particular, a high Sc

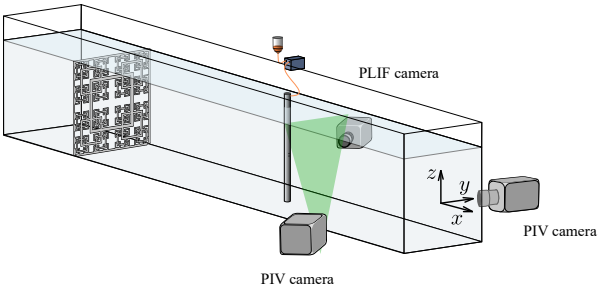

Figure 1: Experimental setup. Note that the origin of the laboratory coordinate system has been moved downstream for clarity.

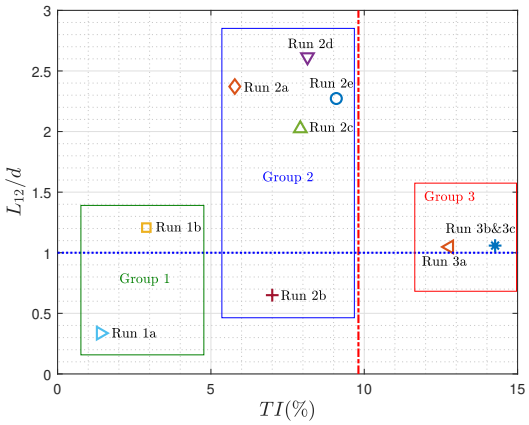

Figure 2: $\{L_{12}, TI\}$ (length-scale - turbulence intensity) parameter space of the freestream turbulence explored. The red vertical line corresponds to the turbulence intensity within the wake for the no-grid case (Run 1a).

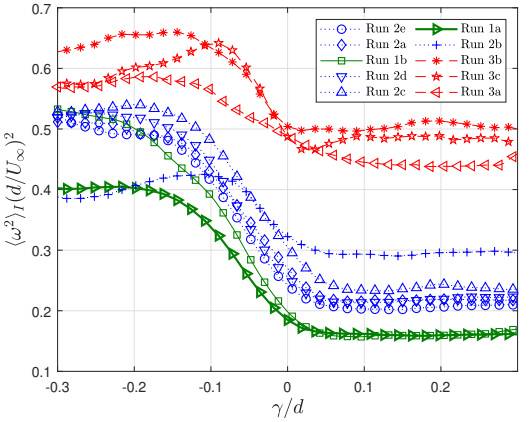

Figure 3: Mean enstrophy conditioned on interface-normal location. $\gamma = 0$ corresponds to the wake boundary with $\gamma > 0$ being the freestream and $\gamma < 0$ being within the wake.

scalar is used to ensure the effects of molecular diffusion are negligible. We thus deploy a combined high-speed particle image velocimetry (PIV) and planar laser induced fluorescence (PLIF) approach. Two experimental campaigns were conducted, one in which planar PIV was used and one in which cinematographic stereoscopic PIV was used (in conjunction with Taylor's hypothesis) to measure all of the three-dimensional terms of (1). A circular cylinder of diameter d is placed in a water flume, such that $Re_d = 4000$, a variable distance downstream of a turbulence generating grid to ensure that the background is fully turbulent. The type of grid and grid - cylinder spacing are varied such that the integral length scale L_{12} and turbulence intensity $TI = u'/U_\infty$, where u' is the r.m.s. velocity fluctuation, of the background turbulence can be independently varied. The experimental setup for the stereoscopic PIV campaign is illustrated in figure 1. Note that the origin of the coordinate system is the centre of the cylinder, however this has been shifted downstream for reasons of clarity in the figure. The PIV cameras interrogate a necessarily small field of view approximately $40d$ downstream of the cylinder (i.e. the wake was fully developed) in order to ensure that the spatial resolution of approximately 3.6η was sufficient to resolve the various terms of (1). The turbulent Reynolds number at this field of view was $Re_\lambda = 94$. Figure 2 shows the explored $\{L_{12}, TI\}$ parameter space of the freestream turbulence. Of particular note are the runs categorised as "group 3" where the TI of the background turbulence is greater than that within the wake (denoted with the solid red line). Full details of the experimental methods, including the identification of the interface location using a threshold on gradient of the PLIF light intensity $|\nabla\phi|$, are given in Kankanwadi & Buxton (2020) and Kankanwadi & Buxton (2022).

RESULTS AND DISCUSSION

First of all we address the zeroth-order question of whether the turbulent/turbulent interface even exists, which has been previously questioned (e.g. da Silva et al., 2014)? Figure 3 shows the mean enstrophy conditioned on normal distance γ from the wake boundary ($\gamma = 0$, analogous to the irrotational boundary for a TNTI) for the various experimental runs considered. In all cases it can be seen that the enstrophy adjusts itself from a fixed level in the freestream ($\gamma > 0$) to some other fixed level within the wake ($\gamma < 0$) over some short distance in a result that is directly analogous to what is observed in a TNTI (e.g. da Silva et al., 2014). This holds true in even the most extreme cases of background turbulence where the TI of the background is greater than that in the wake (group 3). This represents a repeatably observed fluidic discontinuity (independently of the artificially introduced scalar) and thus constitutes proof of the existence of the TTI, even in cases where the TI of the background is comparable (or even greater) than that in the primary turbulent flow.

We verify the existence of the TTI through additional consideration of the two-point statistics of the interfacial region crossing the wake boundary $\gamma = 0$. Figure 4 depicts the correlation of the fluctuating spanwise component of vorticity in the interface-normal direction, $R_{\omega_3'\gamma}$,

$$R_{\omega_3'\gamma} = \frac{\langle \omega_3'(\gamma)\omega_3'(\gamma+r)\rangle}{\sqrt{\langle \omega_3'^2(\gamma)\rangle}\sqrt{\langle \omega_3'^2(\gamma+r)\rangle}}. \qquad (2)$$

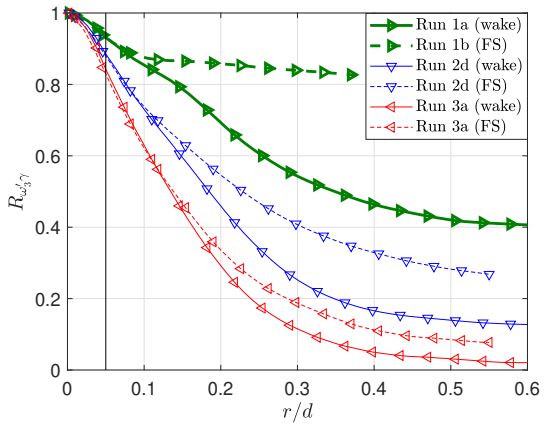

Figure 4: Correlation function for the spanwise vorticity component in the interface-normal direction.

The fixed probe is located $0.05d$ into the freestream side of the wake boundary, i.e. $\gamma = 0.05d$, and r denotes the distance from the fixed probe in the interface-normal direction. Solid lines in the figure represent correlations in which r points in the direction of the wake, whereas dashed lines indicate r pointing into the freestream. In the interests of clarity only one example from each group has been presented in figure 4. As expected, an asymmetric correlation function is observed with more rapid de-correlation witnessed as the moving probe crosses the wake boundary (solid lines), in comparison to a slower de-correlation as the moving probe traverses the freestream (dashed lines). The level of asymmetry between the correlation functions pointing in different directions relative to the interface is seen to drop for cases with increased background turbulence intensity, however this may be expected since more intense turbulence is expected to de-correlate over a physically shorter distance. We thus confirm the existence of a turbulent/turbulent interface where the enstrophy adjusts itself between the levels found on either side of the interface, similarly to a TNTI. We finish by drawing an analogy between the TTI and internal shear layers (across which there is a discontinuity in, and de-correlation of, turbulent statistics) which are thought to be a feature of high-Reynolds number turbulence (e.g. Hunt et al., 2010; Ishihara et al., 2013).

Whilst it is not the intention of this paper to establish a scaling for the identified TTI thickness, it can be useful to represent the thickness of the interface as a function of known turbulent length scales. The vorticity adjustment region of run 1a (our closest approximation to a TNTI) may be estimated to have a thickness of $0.2d$. Using Taylor and Kolmogorov scales calculated for the no-grid case, $0.2d$ is equivalent to approximately 0.7λ and 12.5η. These are in line with the TNTI thicknesses observed in literature (e.g Silva et al., 2018). We also note that the solid and dashed correlations of figure 4, i.e. those pointing towards the wake and the freestream, begin to diverge at $r \approx 0.12d$, i.e. $\approx 0.07d$ into the interface. This corresponds to $\approx 4.5\eta$, which is very close to the widely accepted thickness for the viscous superlayer of a TNTI, although we make no claims as to having identified the viscous superlayer from these correlation functions.

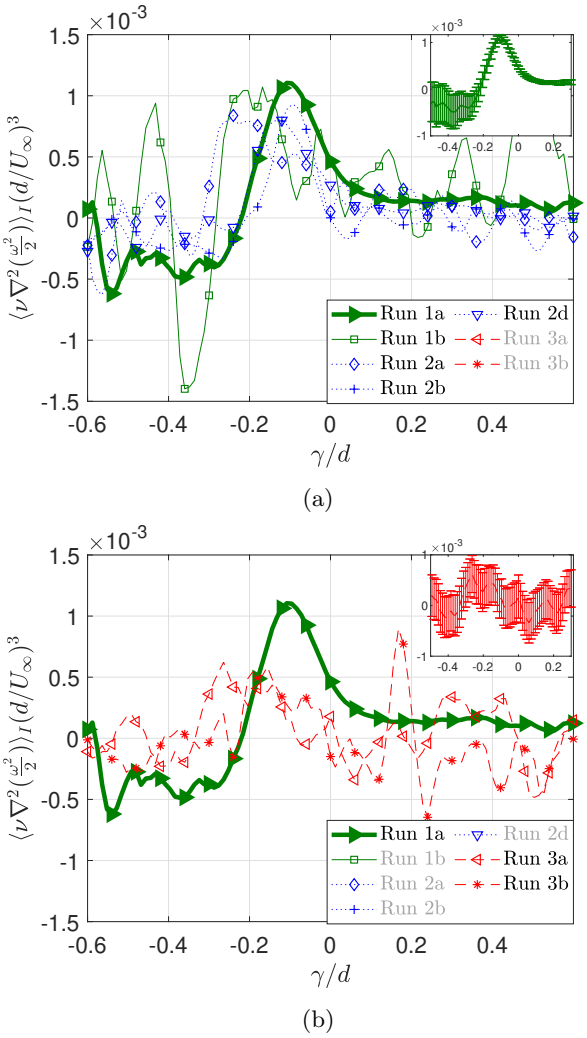

Figure 5: The interface conditioned plot of the viscous diffusion term of (1) for cases in (a) groups 1 & 2 and (b) group 3. The inset displays 95% confidence intervals for the no-grid (a) and run 3a (b) cases.

We now consider the relevant flow physics in the TTI. Since $\omega^2 \neq 0$ on both sides of the TTI, the inertial vortex stretching term $\omega_i s_{ij} \omega_j$ of (1) is no longer constrained to be zero at the wake boundary and so can act as a source term to generate this enstrophy jump. Accordingly, there is no requirement for the viscous diffusion term to be the only source term of (1) at the wake boundary as there is for a TNTI. We therefore seek to determine the role of viscous diffusion in a TTI through consideration of figure 5 which shows the mean viscous diffusion term conditioned on distance from the wake boundary γ for (a) groups 1 and 2 and (b) group 3 (a reminder that these groups are classified based on the turbulence intensity of the background turbulence as shown in figure 2). In both sub-figures the behaviour of the no-grid case, our closest approximation to a TNTI, is presented for comparison as the solid green line. The behaviour of the viscous term from the no-grid case is remarkably similar to results for TNTIs obtained via direct numerical simulation (e.g. Taveira & da Silva, 2014; Watanabe et al., 2014; Silva et al., 2018), acting as a source at the wake (irrotational) boundary and at-

taining a maximum a short distance inside the interface before then acting as a sink and eventually returning to zero, giving us further confidence in our experimental methodology. The viscous diffusion term acts in a similar manner to the no-grid case for runs in groups 1 and 2 with minimal activity in the freestream followed by source-like behaviour in the outer portion of the interface. All cases with background turbulence exhibit increased statistical noise which may be expected due to diminishing sample sizes related to the interface position fluctuating more when exposed to freestream turbulence, often outside of the small-scale PIV field of view. However, even with the increased noise the underlying behaviour can be established for groups 1 and 2. This is not the case for runs that lie in group 3 where all of the similarity to the no-grid case is lost. The level of noise is also greater as the characteristic production peak is no longer distinctly visible.

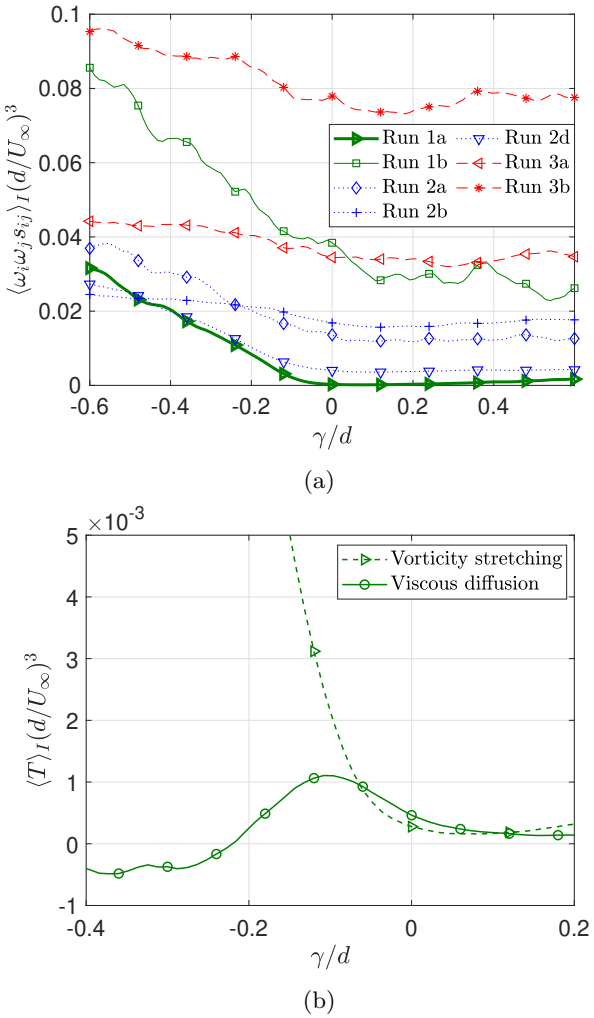

Figure 6: (a) Mean $\omega_i s_{ij} \omega_j$ conditioned on interface-normal location. (b) Zoomed in behaviour of the inertial and viscous source terms of (1) close to the wake boundary for the no-grid case, run 1a.

Figure 6(a) shows the conditional mean (inertial) vorticity stretching term of (1) $\omega_i s_{ij} \omega_j$ as a function of γ. The thick green line is produced from the no-grid case and is thus our closest approximation to a TNTI. Figure 6(b) shows both the conditional mean vorticity stretching term and the conditional mean viscous diffusion term for the no-grid case, zoomed in around the region $\gamma \approx 0$. The behaviour of $\omega_i s_{ij} \omega_j$ also closely follows that reported in literature for TNTIs, with the magnitude of $\omega_i s_{ij} \omega_j$ being smaller than that of the viscous diffusion in the outer-most portion of the interface before exceeding it some short distance away from the wake (irrotational) boundary and then completely dominating in the inner part of the interface (and bulk portion of the flow) (e.g. da Silva et al., 2014; Watanabe et al., 2014). This behaviour is also in accordance with the intuition of Corrsin & Kistler (1955). For all cases with freestream turbulence present in figure 6(a) the vorticity stretching term is non-zero at the wake boundary, since $\langle \omega_i s_{ij} \omega_j \rangle > 0$ is a feature of homogeneous turbulence (Taylor, 1938). However, it is clear that the vorticity stretching term starts to increase at the wake boundary and increases throughout the thickness of the TTI for all cases with freestream turbulence present. In fact, the magnitude of this term dwarfs that of viscous diffusion (c.f. figure 5) and so we conclude that viscosity is an unimportant source of enstrophy amplification in a TTI - a result of some consequence for modelling strategies that frequently model entrainment through diffusion, inspired by the phenomenology of TNTIs.

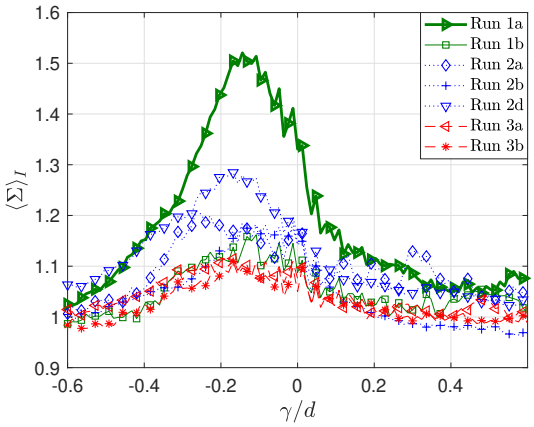

Figure 7: Small-scale anisotropy ratio $\langle \Sigma \rangle$ conditioned on interface-normal location. Values greater than unity correspond to small-scale anisotropy with enhanced velocity gradients normal to the interface.

Our results show that the role of viscosity, in terms of the relative strength of the viscous diffusion term to the inertial vorticity stretching term, is reduced to insignificance in a turbulent/turbulent interface, and that it is this vorticity stretching term that is responsible for the conditional mean enstrophy jump, characteristic of the turbulent/turbulent interface. We now seek to address the origins of this enhanced vorticity stretching term on the wake-side of the TTI only and to determine why a discontinuity in enstrophy exists, with a jump in enstrophy existing even in cases where the TI of the background turbulence exceeds that in-

side the wake. Previous work on TNTIs has identified strong small-scale anisotropy in which the presence of a turbulent interface enhances the interface-normal velocity gradients (e.g. Cimarelli et al., 2015). We now address whether a similar small-scale anisotropy exists in TTIs. To do so we resolve the velocity vector into a (pseudo two-dimensional) interface coordinate system $v = (v_\gamma, v_\xi, v_x)$, where v_γ and v_ξ are the components of velocity normal and parallel to the interface locally (from our planar data), i.e. in the ξ and γ directions, and v_x is the out-of-plane component (which is the streamwise component from our cinematographic stereoscopic PIV experiment). We now define an anisotropy ratio $\langle\Sigma\rangle = \langle(\partial v_\gamma/\partial\gamma)^2/(\partial v_\xi/\partial\xi)^2\rangle$ as a function of γ. Note that the interface-conditioned anisotropy has been calculated two-dimensionally in the transverse $y-z$ plane using only the v and w velocity components. Figure 7 reveals that far away from the interface $\langle\Sigma\rangle$ is unity, symptomatic of turbulence exhibiting small-scale isotropy, but in the TTI region on the wake side only, small-scale anisotropy is introduced with enhanced turbulent strain rates normal to the interface. This is a result that is also mirrored in the turbulent sublayer of TNTIs (e.g. Buxton et al., 2019).

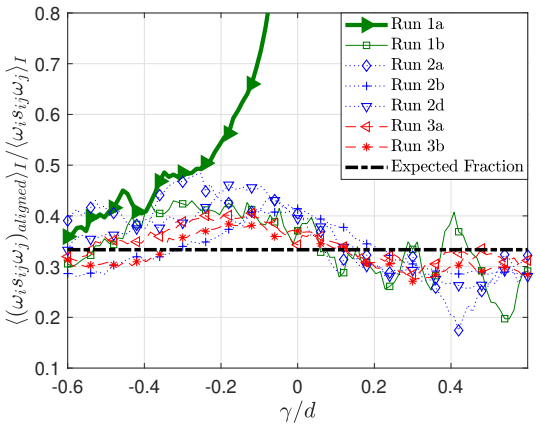

Figure 8: Proportion of overall $\omega_i s_{ij}\omega_j$ contributed by the principal strain rate most closely aligned with the interface-normal direction.

The enhanced strain rates normal to the interface offer a potential explanation for the enhanced enstrophy production yielding the enstrophy jump in TTIs. However, enstrophy production through vorticity stretching depends not only on the magnitudes of the strain-rate tensor and vorticity vector, but also their alignment. This is illustrated in the following decomposition of the vorticity stretching term (Betchov, 1956)

$$\omega_i s_{ij}\omega_j = \sum_{i=1}^{3} \omega^2 s_i (\hat{\omega}\cdot\hat{e}_i)^2 \qquad (3)$$

where s_i are the eigenvalues of s_{ij} with corresponding unit eigenvectors $\hat{e}_i$. (3) illustrates that it is both the magnitude and alignment of the vorticity vector (with respect to the strain rates) that determines $\omega_i s_{ij}\omega_j$. We choose the particular term on the right hand side of (3) for which $\hat{\gamma}\cdot\hat{e}_i$ is maximum, i.e. the term in which the strain rate is best aligned with the interface-normal direction, and plot its contribution to $\omega_i s_{ij}\omega_j$ overall as a function of γ in figure 8. This should reflect the relative contribution of the RHS term of (3) that is best able to exploit the enhanced strain rate normal to the interface, i.e. the small-scale anisotropy. It can be seen that the contribution of this term is $\omega_i s_{ij}\omega_j/3$ far away from the wake boundary (all three terms of (3) contribute equally to $\omega_i s_{ij}\omega_j$) but spikes to larger values at the same locations where the enstrophy jump and enhanced small-scale anisotropy are located. We thus conclude from figure 8 that the vorticity in the wake-side of the TTI is "organised" to take advantage of the enhanced strain rate in the interface-normal direction and produce the enstrophy jump that is characteristic of the TTI.

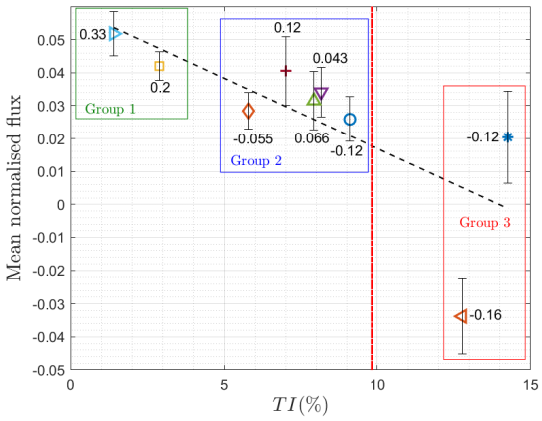

Figure 9: Entrainment mass flux as a function of TI of the background turbulence.

Finally, we explore the effects of background turbulence on the entrainment rate itself into the far wake region, $x \approx 40d$. The entrainment rate is computed by integrating the entrainment velocity v_E along the captured interface within our field of view. Due to the limitations of our planar data we define a normalised entrainment flux as

$$\text{Normalised mass flux} = \frac{1}{dU_\infty}\int v_E \mathrm{d}\xi \qquad (4)$$

where $v_E = v_I - v_0$, i.e. the entrainment velocity is the difference between the local interface velocity v_I and the local fluid velocity v_0. Figure 9 shows that the entrainment mass flux decreases as a function of TI of the background turbulence. Consideration of the probability density functions (PDFs) of the normalised mass flux (with one flux computed from each PIV snapshot) shows that this is largely driven by an increased prevalence of rare, but high-magnitude (i.e. intermittent) detrainment events as the background turbulence intensity is increased (Kankanwadi & Buxton, 2020). It is well known that $\omega_i s_{ij}\omega_j$ is an intermittent quantity in turbulent flows at moderate/high Reynolds number (as is symptomatic of turbulent velocity gradient quantities). We previously showed that the turbulent physics of the

TTI are dominated by $\omega_i s_{ij} \omega_j$ which offers an explanation for why intermittency is a powerful driver of the reduction of entrainment rate as freestream turbulence intensity is increased in the far-wake region.

CONCLUSIONS

We verify the existence of a distinct interface separating the far field of a turbulent wake and a turbulent background; the turbulent/turbulent interface (TTI). The TTI was examined in detail through interface-conditioned statistics of the enstrophy transport equation (1). Unlike for a TNTI, with rotational fluid available in the free-stream side of a TTI the vorticity stretching term is free to contribute to enstrophy production throughout the entire thickness of the interface, including at the wake boundary. Results showed that the magnitude of enstrophy production through the vorticity stretching term dwarfed that of the viscous diffusion term hence it is possible to conclude that in a TTI the role of viscosity is reduced to insignificance. Similarly to a wall in wall-bounded turbulence, the TTI acts to enhance strain-rates in the interface-normal direction close to the boundary. Decomposing the vorticity stretching term into three terms corresponding to the three principal strain directions highlighted that the component most aligned to the interface-normal direction contributes the largest share of enstrophy production on the wake side of the interface. This is indicative of better "organised" vorticity on the wake side that takes advantage of the strong interface-normal strain rates to produce the enstrophy jump observed in a TTI. These results have important implications with regards to modelling entrainment behaviour in a turbulent environment as the role of vorticity stretching is instrumental in the entrainment process, something typically neglected when only considering entrainment from a non-turbulent background. Finally, we show that the presence of freestream turbulence has the effect of reducing the entrainment mass flux relative to a non-turbulent background. This is largely driven by intermittency, with rare but powerful detrainment events becoming more common when the background is turbulent.

Our results lead to open questions regarding the phenomenology of a TTI. The structure of a TNTI is well known, as there are distinct layers in which, respectively, viscous and inertial processes dominate the flow physics. For example, it is possible to claim that the viscous super-layer is bounded between the irrotational boundary and the location where the inertial vorticity stretching term produces a larger share of enstrophy than the viscous term (Taveira & da Silva, 2014). However, these bounds lack any physical relevance when applied to the TTI. It is interesting to note that even with turbulence available in the background, the viscous diffusion term for groups 1 and 2 produces a production peak similar to the no-grid case. Hence, it is possible to raise the question: is this is the remnant of a defunct viscous super-layer? Additionally, with a diminished role of viscosity there is also no longer a relevant physical argument supporting the scaling of the thickness of the TTI with the Kolmogorov length scale.

Lastly, it should be noted that by considering the far wake (i.e. a fully-developed turbulent shear flow) it is assumed that the generality of the study is increased, with the analysis being more applicable to other flows such as jets and even boundary layers. Whilst it is not possible to claim any universality, since that would require experiments conducted over a large range of Reynolds numbers using several flow types, the results are robust within the extensive parametric envelope that was investigated. The considered freestream turbulence conditions had length scales both larger and smaller than the wake-generating object as well as intensities smaller and larger than within the wake.

REFERENCES

Betchov, R.J. 1956 An inequality concerning the production of vorticity in isotropic turbulence. J. Fluid Mech. 1, 497–504.

Buxton, O.R.H., Breda, M. & Dhall, K. 2019 Importance of small-scale anisotropy in the turbulent/nonturbulent interface region of turbulent free shear flows. Phys. Rev. Fluids 4 (3), 034603.

Cimarelli, A., Cocconi, G., Frohnapfel, B. & de Angelis, E. 2015 Spectral enstrophy budget in a shear-less flow with turbulent/non-turbulent interface. Phys. Fluids 27 (12), 125106.

Corrsin, S. & Kistler, A.L. 1955 Free-stream boundaries of turbulent flows. Tech. Rep. NACA Tech. Rep. TN-1244.

Holzner, M & Lüthi, B 2011 Laminar superlayer at the turbulence boundary. Phys. Rev. Lett. 106 (13), 134503.

Hunt, J.C.R., Westerweel, J., Davidson, P.A., Voropayev, S., Fernando, J. & Braza, M. 2010 Thin shear layers – the key to turbulence structure? J. Hydro-Environ. Res. 4 (2), 75–82.

Ishihara, T., Kaneda, Y. & Hunt, J.C.R. 2013 Thin shear layers in high Reynolds number turbulence - DNS results. Flow Turbul. Combust. 91 (4), 895–929.

Kankanwadi, K.S. & Buxton, O.R.H. 2020 Turbulent entrainment into a cylinder wake from a turbulent background. J. Fluid Mech. 905, A35.

Kankanwadi, K.S. & Buxton, O.R.H. 2022 On the physical nature of the turbulent/turbulent interface. J. Fluid Mech. To appear.

da Silva, C.B., Hunt, J.C.R., Eames, I. & Westerweel, J. 2014 Interfacial layers between regions of different turbulence intensity. Annu. Rev. Fluid Mech. 46 (1), 567–590.

Silva, T.S., Zecchetto, M. & da Silva, C.B. 2018 The scaling of the turbulent/non-turbulent interface at high Reynolds numbers. J. Fluid Mech. 843, 156–179.

Taveira, R.R. & da Silva, C.B. 2014 Characteristics of the viscous superlayer in shear free turbulence and in planar turbulent jets. Phys. Fluids 26 (2), 21702.

Taylor, G.I. 1938 Production and dissipation of vorticity in a turbulent fluid. Proc. R. Soc. Lond. A 164 (916), 15–23.

Watanabe, T., Sakai, Y., Nagata, K., Ito, Y. & Hayase, T. 2014 Vortex stretching and compression near the turbulent/non-turbulent interface in a planar jet. J. Fluid Mech. 758, 754–785.